Control-oriented modelling of combustion phasing for a fuel-flexible spark-ignited engine with variable valve timing

Carrie M Hall, Gregory M Shaver, Jonathan Chauvin and Nicolas Petit

International Journal of Engine Research published online 10 April 2012
DOI: 10.1177/1468087412439019

International Journal of ENGINE RESEARCH

Original Article

International J of Engine Research
0(0) 1–16

DOI: 10.1177/1468087412439019
jer.sagepub.com
SAGE

Control-oriented modelling of combustion phasing for a fuel-flexible spark-ignited engine with variable valve timing

Carrie M Hall[1], Gregory M Shaver[1], Jonathan Chauvin[2] and Nicolas Petit[3]

Abstract

In an effort to reduce dependence on petroleum-based fuels and increase engine efficiency, fuel-flexible engines with advanced technologies, including variable valve timing, are being developed. Fuel-flexible spark-ignition engines permit the increased use of ethanol–gasoline blends. Ethanol, an alternative to petroleum-based gasoline, is a renewable fuel, which has the added advantage of improving performance in operating regions that are typically knock limited due to the higher octane rating of ethanol. Furthermore, many modern engines are also being equipped with variable valve timing, a technology that can increase engine efficiency by reducing pumping losses. Through control of valve timings, particularly the amount of positive valve overlap, the quantity of burned gas in the engine cylinder can be altered, eliminating the need for intake throttling at many operating points. However, the presence of elevated levels of in-cylinder burned gas and ethanol fuel can have a significant impact on the combustion timing, such that capturing these effects is essential if the combustion phasing is to be properly controlled.

This paper outlines a physically based model capable of capturing the impact of the ethanol blend ratio, burned gas fraction, spark timing and operating conditions on combustion timing. Since efficiency is typically tied to an optimal CA50 (crank angle when 50% of fuel is burned), this model is designed to provide accurate estimates of CA50 that can be used for real-time control efforts – allowing the CA50 to be adjusted to its optimal value despite changes in ethanol blend and burned gas fraction, as well as the variations in engine thermodynamic conditions that may occur during transients. The proposed control-oriented model was extensively validated at over 500 points across the engine operating range for four blends of gasoline and ethanol. Furthermore, the model was utilized to determine the impact of ethanol blend and burned gas fraction on the CA50, as well as their impact on the optimal spark timing. This study indicated that the burned gas fraction could change the optimal spark timing by over 20° at some operating conditions and that ethanol content could further affect the optimal spark timing by up to 6°. Leveraging the model in this manner provides direct evidence that accounting for the impact of these two inputs is critical for proper spark-ignition timing control.

Keywords

Combustion, spark-ignited engine, fuel-flexible, variable valve timing, combustion phasing

Date received: 20 October 2011; accepted: 2 January 2012

Introduction

Ethanol–gasoline blend-fuelled engines incorporating positive valve overlap (PVO), via variable valve timing (VVT), have the potential to enable the efficient utilization of a nearly CO_2 neutral, domestically available fuel. Ethanol is an attractive option for offsetting dependence on petroleum based fuels; however, the differences in fuel properties between gasoline and ethanol (as summarized in Table 1) can significantly alter engine performance.[1–4] Due to the oxygen content of ethanol, the stoichiometric air–fuel ratio (AFR) of ethanol is substantially different to gasoline. As a result, the air and fuel controllers must target different values for ethanol blends.[1,5–8] Ethanol also has a different laminar

[1]School of Mechanical Engineering, Purdue University, USA
[2]IFP Energies Nouvelles, France
[3]Centre Automatique et Systèmes, École des Mines de Paris, France

Corresponding author:
Carrie M Hall, Ray W. Herrick Laboratories, School of Mechanical Engineering, Purdue University, West Lafayette, IN 47907, USA.
Email: hallcm@purdue.edu

Table 1. Fuel properties.

Property	Gasoline	Ethanol
Molecular formula	$C_{6.16}H_{11.52}$	C_2H_6O
Density (kg/m^3)	744	790
Lower heating value (MJ/kg)	44.1	26.9
Latent heat of vaporization (KJ/kg)	335	903
Octane number	98	129

flame speed than gasoline, such that, combustion timing will differ, depending on the ethanol content of the fuel.

Fortunately, as a result of its higher octane rating, ethanol has a higher resistance to knock than gasoline. While the optimal CA50 (crank angle when 50% of fuel is burned) timing is typically 7–8° crank angle (CA) after top dead centre (TDC),[9] at higher speed/load combinations, spark timing must be retarded when running with gasoline in order to avoid knock. When spark advance is retarded and CA50 no longer occurs at its optimal instant, efficiency is sacrificed. Since ethanol's knock-limited operating region is relatively small,[2,10] such efficiency sacrifices are not typically required. In other words, blends of ethanol can be combusted with more aggressive (i.e. earlier) combustion timings to increase efficiency.

The capability to control PVO (through the use of VVT) on fuel-flexible spark-ignition (SI) engines provides additional efficiency benefits. In studies by Fontana et al.[11] and Cairns et al.,[12] it was found that VVT-enabled PVO provided a 6% and 11% reduction in fuel consumption, respectively, and a theoretical study[13] demonstrated fuel consumption reductions of up to 13%. The aforementioned reductions were realized by reducing the extent to which throttling is required. More specifically, the air and fuel controllers of an SI engine, such as that pictured in Figure 1, keep the AFR at a desired value (typically the stoichiometric AFR in order to allow the three-way catalyst to properly reduce emissions). In order to maintain the desired AFR, throttling is required at part-load; however, throttling causes significant decreases in engine efficiency. On conventional engines with fixed valve timings, throttling to maintain a desired air flow is unavoidable, but engines with VVT can avoid some of these throttling losses.[11,12,14–16] Instead of throttling to reduce the volume of incoming fresh air, some of the fresh air can be displaced by increasing the mass of in-cylinder combustion products (i.e.'burned gas') through the use of PVO. Specifically, valve timings can be varied to change the extent of valve overlap. Figures 2 and 3 show examples of variations in valve overlap. When no overlap occurs, the burned gases present in the cylinder are residual exhaust gases; however, when overlap occurs, exhaust gases can enter the intake manifold (IM) displacing some of the fresh air. While changing the amount of burned gases present can reduce the need for throttling, the addition of burned gases serves to slow flame propagation and directly impacts the rate at which fuel burns.[12] As VVT is becoming increasingly common on SI engines, its impact on the gas exchange process and combustion phasing must be considered.

Due to the impact of the gasoline–ethanol blend ratio and burned gas fraction (BGF) on combustion timing, adaptation in ignition control is required. A conventional ignition controller dictates a spark timing that allows an optimal combustion timing to be achieved. Spark timing is commonly dictated by using static look-up tables. In steady state, these look-up tables provide a spark timing that ensures that the combustion timing (CA50) occurs at its optimal timing. However, if the same look-up tables for ignition control are used for gasoline, ethanol and gasoline–ethanol blends, engine performance will be suboptimal when running any blend fraction of ethanol,[1,4] and therefore, it is essential to take fuel type into consideration when dictating desired set points. One method of achieving this is by adding additional look-up tables to be used for different fuel blends; however, since fuel-flexible spark-ignition (SI) engines commonly run blends of gasoline and ethanol of up to 85% ethanol, adding look-up tables for all possible fuel blends would be quite intensive. Furthermore, the impact of BGF variations would also have to be incorporated in the look-up tables.

An alternative is to use model-based control of CA50 instead of relying extensively on look-up tables. Specifically, a physically based, control-oriented model that accurately estimates the CA50 for various fuel blends and BGFs could be used to synthesize either feedback or feedforward control algorithms. This paper outlines the development and validation of such a model that is capable of providing cylinder-specific, cycle-to-cycle estimates of CA50 during engine operation. While a number of models[17–23] and engine simulation software packages (WAVE, GT-Power) have been created that capture combustion phasing for conventional SI engines to the best of our knowledge, few of these include PVO effects and only that by Bougrine et al.[20] includes ethanol blend impacts. In addition, all of the aforementioned models and simulation packages are more complex than is desirable for controller synthesis. The model presented in this work differs from previously developed models and available software in that it is computationally efficient and control amenable.

The model detailed in this paper is based on the general physical relationships that govern the gas exchange, compression and flame-propagation processes. Since VVT-enabled PVO is becoming increasingly common on SI engines, this capability is also taken into consideration in the gas exchange process. The details of this model are given and the model is validated for four different fuel blends at over 500 operating points, including a wide variety of speed/load conditions over the engine operating range of the engine, as well as variation in spark timing and valve overlap.

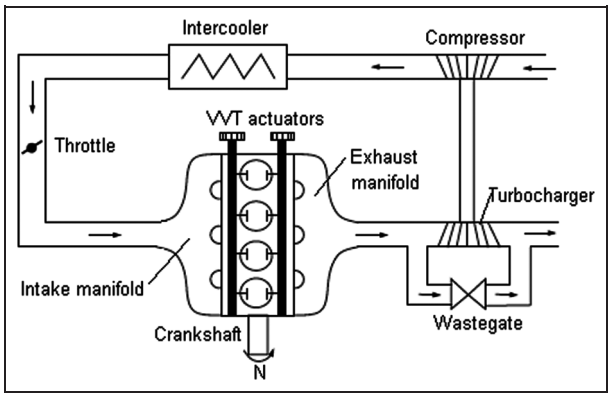

Figure 1. Diagram of SI engine with VVT and turbocharger.

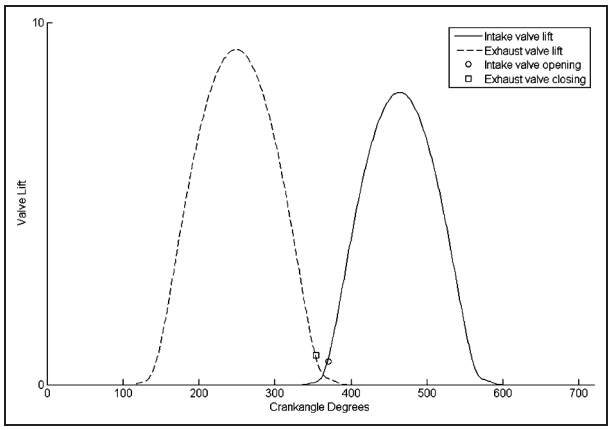

Figure 2. Intake and exhaust valve lifts for cases with no valve overlap.

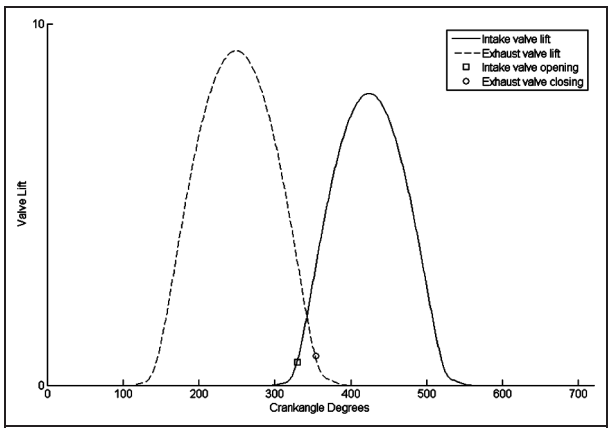

Figure 3. Intake and exhaust valve lifts for cases with valve overlap.

Combustion phasing model

Since the model is designed to be used for control of combustion phasing, it is desirable to capture the underlying dynamics of the system in a manner that is representative, but can be used for real-time estimation and control of CA50 on a fuel-flexible engine with VVT. Combustion phasing could be determined using an in-cylinder pressure measurement, but at this time, such pressure transducers are not commonly used on production engines. While an in-cylinder pressure measurement could be used with the model for control, this model is not dependent on such a pressure measurement and uses only available on-engine sensor measurements to provide accurate estimates of the timing of combustion phasing. The sensor measurements that are commonly available and are utilized in this model are the following:

- engine speed (N)
- spark ignition timing (SIT)
- injected fuel mass (M_{fuel})
- intake manifold pressure (P_{IM})
- intake manifold temperature (T_{IM})
- exhaust manifold pressure (P_{EM})
- exhaust manifold temperature (T_{EM})

On engines with VVT, the commanded valve opening and closing timings will also be used. In addition, to capture the effects of ethanol content on the combustion phasing, the ethanol blend fraction of the fuel must also be either measured or estimated. A number of studies have developed methods of ethanol blend fraction estimation.[1,6,7,24–25]

In order to compute the CA50, the model is comprised of three phases: gas exchange, compression and flame propagation, as shown in Figure 4. The dynamics of these processes are captured by physically based equations, as described in the following sections.

The notation used in this paper is shown in Appendix 1.

Model assumptions

In this model, it is assumed that the in-cylinder mixture is homogenous. After combustion begins, fuel is burned in a thin reaction zone that separates the burned and unburned regions in the cylinder. A pressure

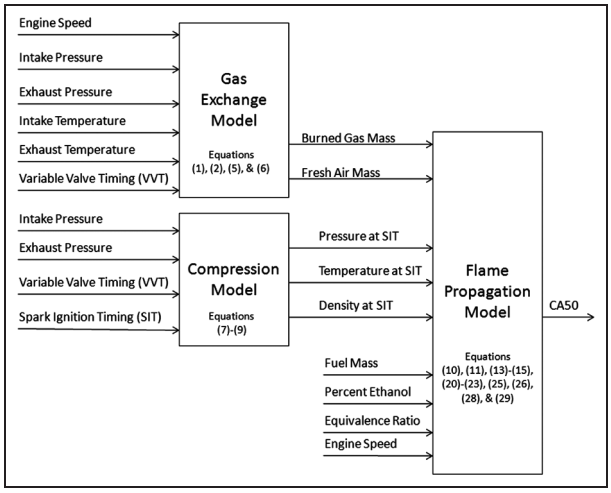

Figure 4. Model diagram.

equilibrium is assumed between the burned and unburned regions.

Gas exchange modelling

In order to capture the dynamics of combustion phasing, it is crucial to have an accurate estimate or measurement of the contents of the cylinder at intake valve closing (IVC). The mixture in the cylinder will be made up of fresh air, residual and reinducted exhaust gases, and fuel. The mass of fuel entering into the cylinder is controlled by the existing engine fuelling control and thus, is known. However, the mass of fresh and burned gases in the cylinder must be calculated from appropriate physically based models. The fuel-flexible engine considered in this work is also equipped with VVT. With a VVT system, it is possible to alter the intake and exhaust valve opening and closing such that both the intake and exhaust valves are open for a period of time. This valve overlap can significantly influence the amount of fresh air and burned gases present in the engine cylinder at IVC.

Fresh air mass. In order to calculate the mass of fresh air, a previously developed cylinder filling model[27,28] for an engine with VVT is used. This model estimates fresh air flow as

$$M_{fresh} = \alpha_1 \frac{P_{IM} \cdot V_{IVC}}{R \cdot T_{IM}} - \alpha_2 \frac{OF}{N} \quad (1)$$

where OF is an overlap factor, N is the engine speed, α_1 is a look-up map, which is a function of engine speed and IM pressure, and represents the volumetric efficiency, and α_2 is also a look-up map as a function of engine speed and IM pressure. The first term on the right-hand side of equation (1) represents the total mass in the cylinder at IVC, and the second term represents the aspirated mass from the exhaust. This model has been previously validated.[27,28]

The α_1 and α_2 used in this study and developed as specified by Leroy et al.[27,28] are shown in Figures 5 and 6. α_1 represents the volumetric efficiency and thus varies slightly across the engine operating range, indicating lower volumetric efficiencies for this particular engine at lower speeds and loads. The α_2 value may be positive or negative depending on whether the exhaust mass is flowing into the cylinder or fresh air is being driven out to the exhaust manifold.

Burned gas mass. The burned gases present in the cylinder are composed of residual exhaust gas as well as possible backflow from the exhaust manifold. While external exhaust gas recirculation (EGR) is becoming increasingly common, it was not present on the engine considered in this work. However, the effects of external EGR could be added to the model, but would require accurate estimates or measurements of the EGR mass. Valve overlap is considered directly in the model, while modulation of valve lift, exhaust valve opening (EVO) and exhaust valve closing (EVC) are not considered. On the engine considered here, variation in valve overlap was achieved through modulation of the intake valve timing only, and variation in valve motion was not considered in this study since the engine utilized had only the capability of changing valve timing not valve lift profile.

In cases where there is negative valve overlap (NVO), EVC occurs before intake valve opening (IVO), as shown in Figure 2, and the total mass of burned gas is only due to the residual exhaust gas that is trapped in the cylinder at EVC. The mass of burned gas can therefore be found by applying the ideal gas law as shown in equation (2) with the assumption that the pressure and temperature in the cylinder at EVC are the same as the conditions in the exhaust manifold,

$$M_{bg,NVO} = \frac{V_{EVC} \cdot P_{EM}}{R \cdot T_{EM}} \quad (2)$$

When IVO occurs prior to EVC (Figure 3), residual gases as well as backflow and scavenging must be considered. In cases with PVO, the residual gas mass can be calculated using the ideal gas law as

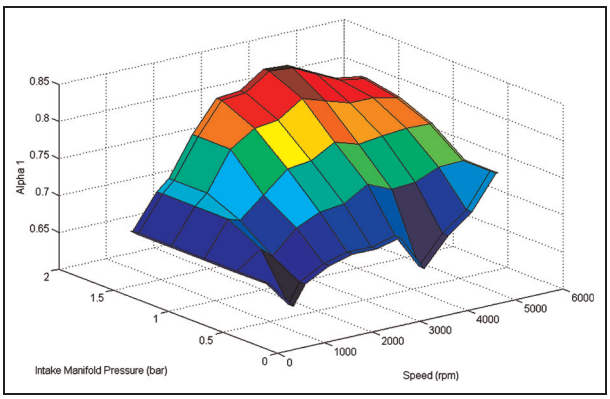

Figure 5. Map of α_1.

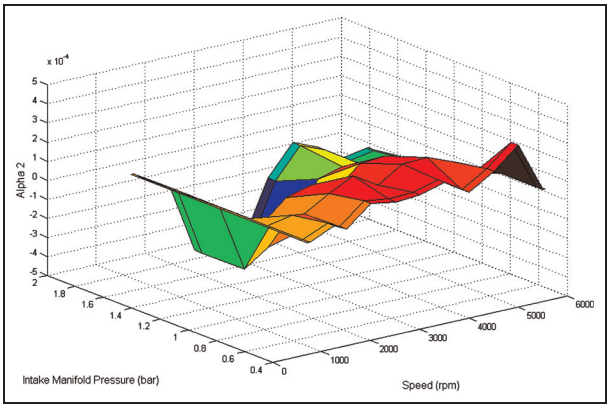

Figure 6. Map of α_2.

$$M_{res} = \frac{V_{IVO} \cdot P_{EM}}{R \cdot T_{EM}} \quad (3)$$

In the period of time between IVO and EVC, gases can flow between the IM, the engine cylinder and the exhaust manifold (EM). Any residual exhaust gas that is expelled into the IM will be reinducted during the intake stroke. In addition, depending on the placement of IVO and EVC and the pressure differential across the engine, residual gas may flow into the exhaust manifold or exhaust gas from the exhaust manifold may re-enter the cylinder (this is commonly referred to as backflow). The engine used in the study had an IVO and EVC that always occurred before TDC, and thus mass is always lost from the cylinder during valve overlap. If IVO and EVC occurred after TDC, the piston would be moving downward during valve overlap, and exhaust gases could be reinducted back into the cylinder. However, since valve overlap always occurs before TDC on this engine, the piston is moving upward, and volume is being forced out of the cylinder during valve overlap. The portion of residual gas that is lost to the intake and exhaust manifolds during this time of valve overlap can be found using the ideal gas law. The fraction of this residual mass that exits the exhaust manifold is assumed to be proportional to the pressures in the intake and exhaust manifolds. Thus, in a similar method as that used by Kocher et al.,[29] these backflow effects are captured by

$$M_{backflow} = \frac{P_{IM}}{P_{IM} + P_{EM}} \cdot \frac{(V_{EVC} - V_{IVO}) \cdot P_{EM}}{R \cdot T_{EM}} \quad (4)$$

Combining equations (3) and (4), the total burned gas mass in the case of valve overlap is

$$M_{bg,\,PVO} = \frac{V_{IVO} \cdot P_{EM}}{R \cdot T_{EM}} + \frac{P_{IM}}{P_{IM} + P_{EM}} \cdot \frac{(V_{EVC} - V_{IVO}) \cdot P_{EM}}{R \cdot T_{EM}} \quad (5)$$

Equations (1), (2), (5) and the controlled fuelling mass provide the composition of the cylinder mixture at IVC. The BGF can then be computed by

$$Y_{bg} = \frac{M_{bg}}{M_{bg} + M_{fresh}} \quad (6)$$

where M_{fresh} is given by equation (1) and M_{bg} is given by either equation (2) or (5), depending on the valve overlap.

Compression modelling

After the contents of the cylinder (i.e. the burned gas mass and fresh air mass) are computed, the evolution of the temperature and pressure of these contents from IVC to SIT must be computed. In this phase, polytropic compression with a polytropic coefficient (n) of 1.29 is assumed. Furthermore, the temperature and pressure at IVC are assumed to be approximately equal to those in the IM. The conditions at SIT can be found by equations (7) and (8).

$$P_{SIT} = P_{IM} \cdot \left(\frac{V_{IVC}}{V_{SIT}}\right)^{n} \quad (7)$$

$$T_{SIT} = T_{IVC} \cdot \left(\frac{V_{IVC}}{V_{SIT}}\right)^{n-1} \quad (8)$$

The temperature at IVC, T_{IVC}, is given by

$$T_{IVC} = Y_{bg} \cdot T_{EM} + (1 - Y_{bg}) \cdot T_{IM} \quad (9)$$

in order to take into account the effect of burned gases on the initial temperature at IVC.

Flame-propagation modelling

Shortly after a spark is applied, the mixture will begin to burn. In order to estimate the time it takes for the fuel to burn, it is necessary to predict the manner in which the flame propagates.

Inputs. In addition to the pressure and temperature at SIT determined by equations (7) and (8) in the compression phase of the model, it is also necessary to know the mass fraction of fuel in the cylinder and the initial density of the cylinder contents at SIT. Since the in-cylinder contents are assumed to be homogenous, the mass fraction of fuel in the unburned zone is

$$Y_{fuel,\,u} = \frac{M_{fuel}}{M_{fuel} + M_{fresh} + M_{bg}} \quad (10)$$

The initial density at SIT is

$$\rho_{u,\,SIT} = \frac{M_{fuel} + M_{fresh} + M_{bg}}{V_{SIT}} \quad (11)$$

Equations (7) to (11) provide the thermodynamic conditions at SIT and give the initial conditions for the flame-propagation model.

Mass fraction of fuel burned. Following SI, the rate at which fuel is burned can be described by

$$\frac{dm_{fuel}}{dt} = \rho_u \cdot U_{turb} \cdot \overline{A} \quad (12)$$

where ρ_u is the density in the unburned region, U_{turb} is the turbulent flame speed, and $\overline{A}$ is the mean flame surface area.[30] Note that since the mixture is assumed to be homogenous, this rate of fuel burn will be the same as the mixture burn rate.

Alternatively, the fraction of fuel burned (x_{fuel}) is captured by the following relationship, which is derived from equation (12),

$$\frac{dx_{fuel}}{dt} = \frac{1}{M_{fuel}} Y_{fuel,\,u} \cdot \rho_u \cdot U_{turb} \cdot \overline{A} \quad (13)$$

The total mass of fuel injected (M_{fuel}) is known and the mass fraction of fuel (equation (10)) throughout the unburned zone is considered uniform due to the

homogeneity assumption. In order to evaluate equation (13), ρ_u, U_{turb} and $\overline{A}$ must also be determined.

Unburned density and temperature. In order to calculate the evolution of the temperature and density in the unburned zone, polytropic compression of the unburned gases is assumed,[9,31,32] as captured by equations (14) and (15),

$$T_u = T_{u,SIT} \cdot \left(\frac{P}{P_{SIT}}\right)^{\frac{n-1}{n}} \tag{14}$$

$$\rho_u = \rho_{u,SIT} \cdot \left(\frac{P}{P_{SIT}}\right)^{\frac{1}{n}} \tag{15}$$

The unburned density (ρ_u) is required by equation (13), and the temperature in the unburned region will be required for computation of the flame speed.

Heat transfer may affect this unburned temperature and the impact of heat transfer is likely strongly dependent on the engine speed. However, this model uses the estimated unburned temperature solely in the calculation of turbulent flame speed and the relationship for turbulent flame speed does include several tuning factors that provide a dependence on engine speed. Thus, this effect of heat transfer on temperature and therefore flame speed is most likely being captured by the tuning for the turbulent flame speed model as detailed in the section on turbulent flame speed.

In-cylinder pressure. The in-cylinder pressure and heat-release analysis is modelled based on first principles. While the approach is straightforward, it appears to capture the burn rate accurately and similar physics-based methods have been extensively used in other control-oriented models (such as those by Hillion et al.[31,32] and Koeberlein[33]) with promising results.

The change in pressure in the flame-propagation stage can be deduced from the First Law of Thermodynamics

$$\frac{dE}{dt} = \frac{dQ}{dt} - \frac{dW}{dt} + \sum \dot{m}_i h_i \tag{16}$$

which can be rewritten for a closed system as

$$\frac{dU}{dt} = \frac{dQ}{dt} - P\frac{dV}{dt} \tag{17}$$

Assuming constant specific heats and an ideal gas, equation (17) becomes

$$(\gamma - 1)\frac{dQ}{dt} = \gamma \cdot P\frac{dV}{dt} + V\frac{dP}{dt} \tag{18}$$

Furthermore, the heat addition due to combustion of the fuel can be expressed as

$$\frac{dQ}{dt} = M_{fuel} \cdot Q_{LHV} \cdot \frac{dx_f}{dt} \tag{19}$$

in which Q_{LHV} is the lower heating value of the fuel used.

Plugging equation (19) into equation (18) yields

$$(\gamma - 1) \cdot M_{fuel} \cdot Q_{LHV} \cdot \frac{dx_{fuel}}{dt} = \gamma \cdot P\frac{dV}{dt} + V\frac{dP}{dt} \tag{20}$$

which is used to evaluate the evolution of in-cylinder pressure following SIT.[32]

Mean flame surface. The mean surface of the flame is modelled[19] as a sphere at the beginning of combustion as

$$\overline{A} = 4 \cdot \pi \cdot (r_{flame})^2 \tag{21}$$

where

$$r_{flame} = \sqrt[3]{\frac{3 \cdot V_b}{4 \cdot \pi}} \tag{22}$$

in which V_b is the burned volume given by

$$V_b = V - V_u = V - \frac{1 - x_{fuel}}{\rho_u} \cdot (M_{fuel} + M_{fresh} + M_{bg}) \tag{23}$$

The derivation of equation (23) is as follows

$$\begin{aligned} V_b &= V - V_u \\ &= V - \frac{M_u}{\rho_u} \\ &= V - \frac{M_{fuel} - m_{fuel}}{Y_u} \cdot \frac{1}{\rho_u} \\ &= V - \frac{M_{fuel} - m_{fuel}}{Y_u} \cdot \frac{1}{\rho_u} \\ &= V - \frac{M_{fuel} - m_{fuel}}{M_{fuel}} \cdot \frac{M_{fuel} + M_{fresh} + M_{bg}}{\rho_u} \\ &= V - (1 - x_{fuel}) \cdot \frac{M_{fuel} + M_{fresh} + M_{bg}}{\rho_u} \end{aligned} \tag{24}$$

where M_{fuel} is the total injected fuel mass and m_{fuel} is the mass of fuel burned. The evolution of the burned gas volume is calculated based on the difference between the total in-cylinder volume and the unburned gas volume. The volume of the unburned gases will be impacted not only by the spread of the flame, but also by compression and expansion, as well as the heat released by combustion. As a result of the pressure rise, the temperature and density in the unburned zone will increase (equations (14) and (15)). As long as the temperature and density of the unburned zone is captured accurately, the unburned volume should be correct and since the total in-cylinder volume is known and constant, the burned volume (found as the difference between total in-cylinder volume and unburned volume) should also be accurate.

Figure 7 demonstrates the mean flame surface model used.

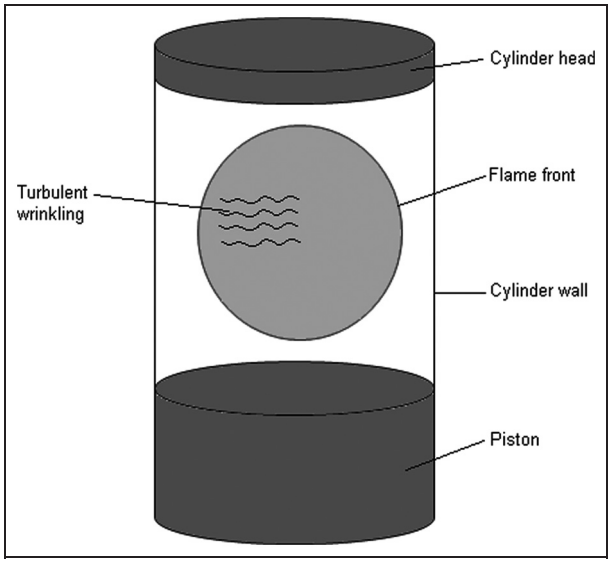

Figure 7. Mean flame surface area model.

After the flame reaches the piston head, the flame progressively becomes a cylinder and the flame area is calculated by equations

$$\overline{A} = 2 \cdot \pi \cdot (r_{flame}) \cdot \delta l \tag{25}$$

$$r_{flame} = \sqrt{\frac{V_b}{\pi \cdot \delta l}} \tag{26}$$

The distance between the cylinder head and the piston is δl.

Turbulent flame speed. The turbulent flame speed, U_{turb}, has been shown to be proportional to the intensity of turbulence in-cylinder and the laminar flame speed. A number of factors including valve overlap and spark timing, as well as in-cylinder swirl and tumble, can have an impact on the turbulence intensity. However, researchers at the University of Michigan[34] have demonstrated that the main driver for in-cylinder turbulence is engine speed and that other factors had only minor effects. Therefore, in an effort to keep the model control amenable, turbulence intensity is modelled solely as a function of engine speed. While a more complex model may improve performance slightly, there did not appear to be a significant detrimental impact due to considering only the major driver of turbulence (engine speed).

Thus, turbulent flame speed is expressed as

$$U_{turb} = f \cdot U_L \tag{27}$$

in which f is a turbulence-enhancement factor that is proportional to engine speed and U_L is the laminar flame speed.[34–36] The laminar flame speed is obtained by

$$U_L = U_{L,0}\left(\frac{T_u}{T_{amb}}\right)^{\alpha}\left(\frac{P}{P_{amb}}\right)^{\beta}(1 - 2.06 \cdot Y_{bg}^{0.75}) \tag{28}$$

$$U_{L,0} = Z \cdot W \cdot \phi^{\eta} \cdot e^{-\xi \cdot (\phi - 1.075)^2} \tag{29}$$

Table 2. Values for constants in laminar flame speed.

Z	$1 \cdot (1 - V_E) + 1.1 \cdot V_E$
W	0.4658
η	0.3
ξ	4.48
α	0.9
β	−0.05

in which Z is fuel dependent and W, η, ξ, α, and β are fuel independent. The mass fraction of burned gases is Y_{bg}. This relationship was developed by Bayraktar,[37] Gulder,[38] Metghalchi and Keck,[39] Bonatesta and Shayler,[40] Syed et al.[41] and Lindström et al.[42] The values for Z, W, η, ξ, α, and β are given in Table 2, in which V_E is the volume fraction of ethanol in the fuel. These constants were tuned for this model but are in close agreement with studies by Syed et al.,[41] Bayraktar[37] and Lindström et al.[42] The linear dependance of laminar flame speed on ethanol blend is captured by Z. While Gülder created a laminar flame speed correlation for ethanol blends[43] that has been used extensively, more recent studies (which have focused on a broader range of ethanol blends, pressures and temperatures) have shown more linear increases in flame speed with respect to ethanol content.[41,44,45] In agreement with the studies of Syed et al.,[41] Broustail et al.[44] and Hara and Tanoue,[45] as well as the trends observed in this study, a linear correlation for Z was used that corresponds to a 10% increase in laminar flame speed at E100.

The turbulent flame speed is then calculated by

$$U_{turb} = (a \cdot N + b) \cdot U_{L,0}\left(\frac{T_u}{T_{amb}}\right)^{\alpha}\left(\frac{P}{P_{amb}}\right)^{\beta} \left(1 - 2.06 \cdot Y_{bg}^{0.75}\right) \tag{30}$$

where a and b are constants of 0.0025 and 3.4, respectively.

Model summary

This flame-propagation model is physically based and generalizable to different engine architectures. It also takes into account the ethanol blend ratio and in-cylinder burned gas. The complexity of the model is kept to a minimum in order to allow the model to be used for control purposes. The entire flame-propagation model is captured by the following two-state model, in which the states are the fraction of fuel burned (x_{fuel}) and the in-cylinder pressure. The first state equation is obtained by substituting equations obtained by combining equations (10), (11), (14), (15) and (30) into equation (13), yielding

$$\frac{dx_{fuel}}{dt} = \frac{1}{V_{SIT}} \cdot \left(\frac{T_u, SIT}{T_{amb}}\right)^{\alpha} \cdot \left(\frac{P^{(1+(n-1)\cdot\alpha)/n+\beta}}{P_{SIT}^{(1+(n-1)\cdot\alpha)/n} \cdot P_{amb}^{\beta}}\right) \cdot (a \cdot N + b) \cdot U_{L,0} \cdot \left(1 - 2.06 \cdot Y_{bg}^{0.75}\right) \cdot \overline{A} \tag{31}$$

Table 3. Engine specifications.

Number of cylinders	4
Compression ratio	10.55
Bore (mm)	82.7
Stroke (mm)	93
Connecting rod length (mm)	144
Engine displacement (l)	2.1

Table 4. Range of variation for engine speed, IM pressure, valve overlap and SIT.

Variable	Minimum	Maximum
Engine speed (r/rmin)	750	5500
Intake manifold pressure (bar)	0.4	2.2
Valve overlap (CA)	−16	24
SIT (before TDC)	−12	61

in which temperature and pressure at SIT can be determined by equations (7) to (9) and values for $U_{L,0}$ and Y_{bg} are given by equations (29) and (6), respectively.

The second state equation is found by rearranging equation (18) to solve for the rate of change in pressure as captured by equation (32).

$$\frac{dP}{dt} = \frac{\gamma - 1}{V} \cdot M_{fuel} \cdot Q_{LHV} \cdot \frac{dx_{fuel}}{dt} - \gamma \cdot P \frac{dV}{dt} \qquad (32)$$

Model validation

The previous section outlined all of the equations necessary to describe the gas exchange, compression and flame-propagation models, as illustrated in Figure 4. Experimentation to validate the model was conducted on a Renault F4RT 2.1 l engine with VVT on the intake valves. Variation in valve overlap on this engine was achieved through modulation of the intake valve timing only. The engine is port-fuel injected and turbocharged. The specifications for this engine are given in Table 3.

The model was validated at over 500 operating points consisting of varying combinations of speed, IM pressure, valve overlap, SIT and ethanol blend fraction. In this study, valve overlap was accomplished by altering the intake timing, as shown in Figures 2 and 3. The fuels considered in the study include E0 (gasoline), E5 (5% ethanol / 95% gasoline), E40 (40% ethanol / 60% gasoline), and E85 (85% ethanol / 15% gasoline). Engine speed, IM pressure, valve overlap and SIT were varied over the ranges shown in Table 4.

As shown in Figure 8, the operating points at which the model was validated cover a variety of speed/load conditions with all four fuel blends.

Recall that a separate submodel (equation (1)) is used for fresh air flow. In order to confirm the validity of this fresh air flow model for the data used in this analysis, the model prediction was compared to experimental values at the 500 points across the engine map

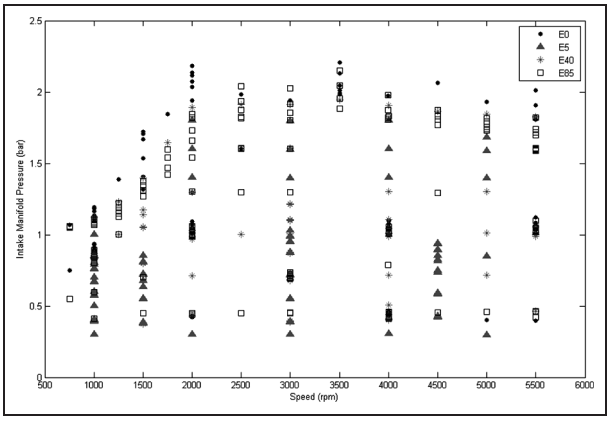

Figure 8. Region over which the model was validated.

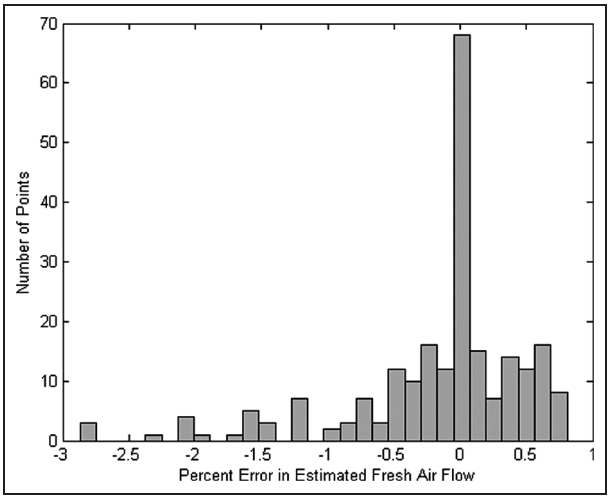

Figure 9. Percent error between the estimated and experimental fresh air flow.

considered in this validation effort, and the percentage error was very small, as shown in Figure 9 giving confidence that this submodel captures the fresh air flow accurately.

Since this model is designed to be used for control of CA50, it is crucial that the model accurately predicts CA50 for a wide variety of conditions. The overall accuracy of the model is demonstrated in Figure 10, in which the model's predictions for CA50 are compared to the experimental values at all the points considered (shown in Figure 8). The black lines on this figure represent ±2 CA from the experimental values and the grey lines represent ±4 CA from the experimental values. While some scatter is observed, at the majority of the data points, the model predicts the CA50 fairly accurately. Another way of investigating the model's accuracy is to examine its ability to properly predict the fuel burn rate from SIT to CA50. Figure 11 shows that the model accurately captures the time from SI until CA50. Note that in Figure 11, the black lines represent ±10% of the experimental values.

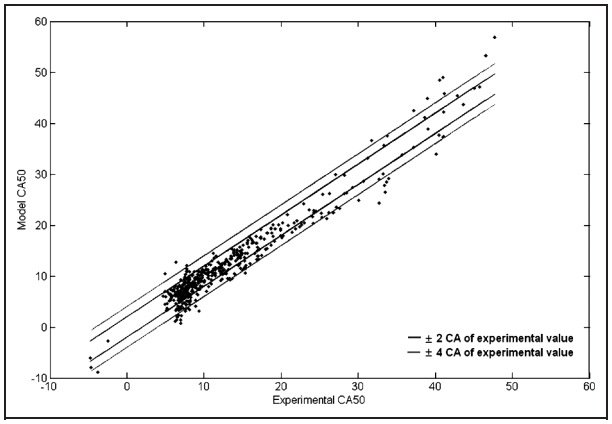

Figure 10. Comparison between experimental value and model prediction for CA50 at over 500 points.

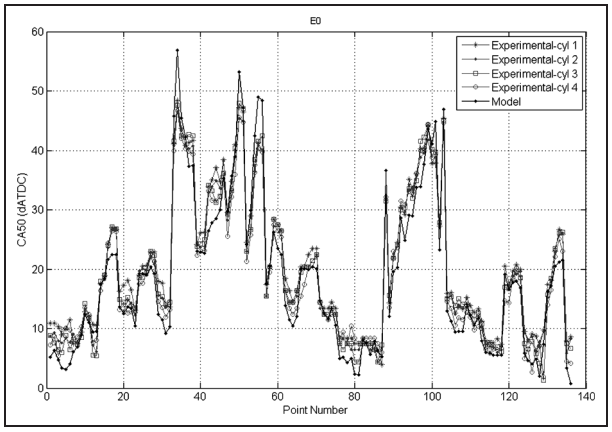

Figure 12. Model prediction of CA50 with E0.

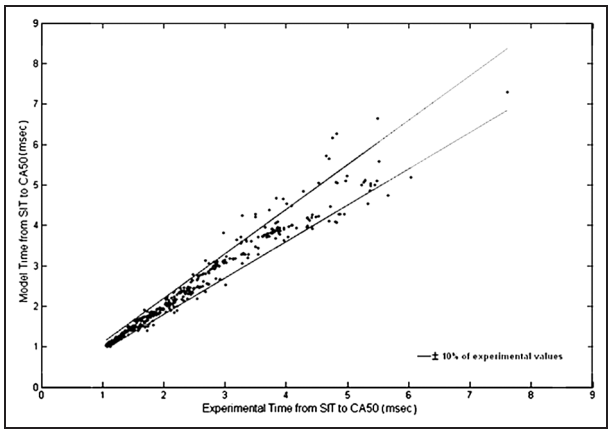

Figure 11. Comparison between experimental value and model prediction for time between SIT and CA50 at over 500 points.

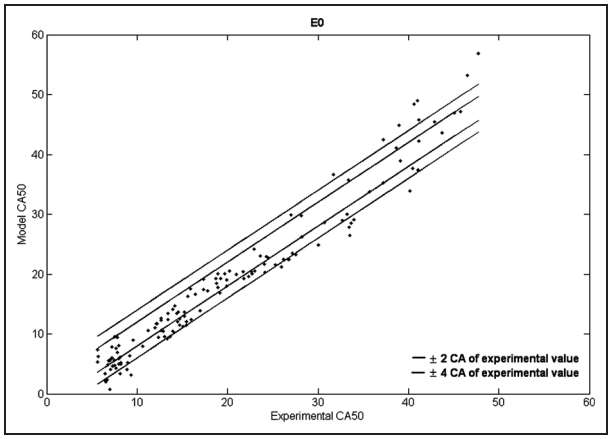

Figure 13. Comparison between average experimental value and model prediction for CA50 with E0.

In order to further investigate the validity of the model, the model accuracy will be considered separately for each of the four fuel blends. Figure 12 demonstrates model prediction for E0 (gasoline). The overall trends are captured well, and absolute values are also captured for most cases. Note that here the experimental values for CA50 from each of the four cylinders are shown. The model accuracy is further demonstrated in Figure 13, where the model prediction is compared to the average experimental CA50. Additional details regarding the variation in speed, intake and exhaust manifold temperature and pressure, fresh air mass, spark advance, and valve overlap for the E0 points are given in Appendix 2.

Similarly, prediction at E5 is also accurate, as demonstrated in Figures 14 and 15. Data for CA50 from all four cylinders was not available for the E5 data set. Only the average CA50 is shown.

The results for E40 are shown in Figures 16 and 17. As with the E5 data set, only the average experimental CA50 was available for comparison with the model.

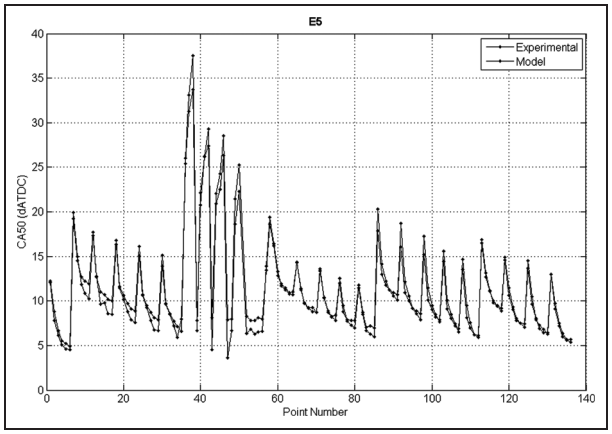

Figure 14. Model prediction of CA50 with E5.

Figures 18 and 19 demonstrate the accuracy of the model predictions for CA50 at a variety of conditions with E85. Experimental values for CA50 from all four cylinders are shown for this data set. Details concerning the variation of the input parameters for the E5, E40, and E85 data sets are given in Appendix 2.

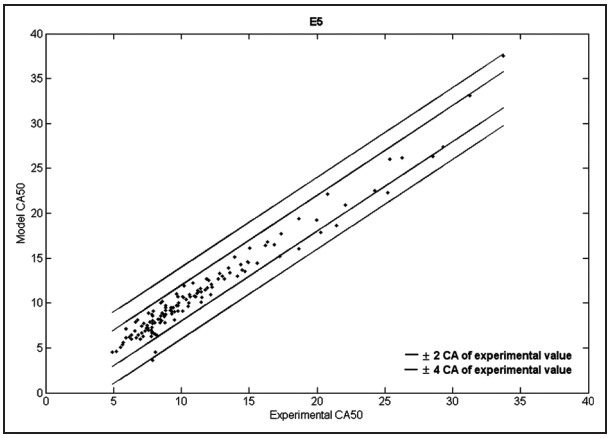

Figure 15. Comparison between average experimental value and model prediction for CA50 with E5.

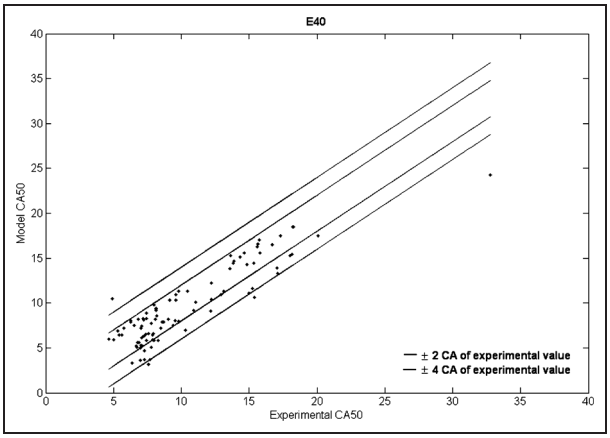

Figure 17. Comparison between average experimental value and model prediction for CA50 with E40.

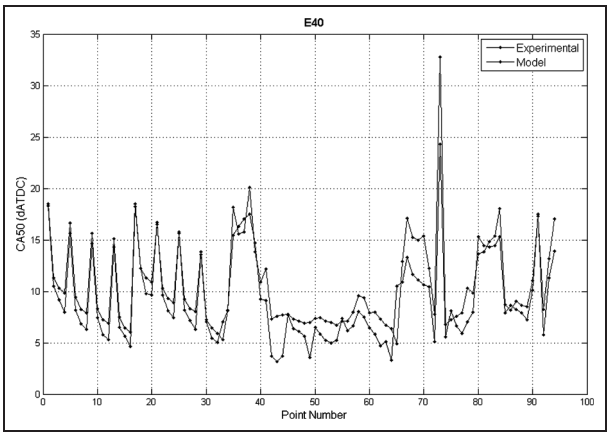

Figure 16. Model prediction of CA50 with E40.

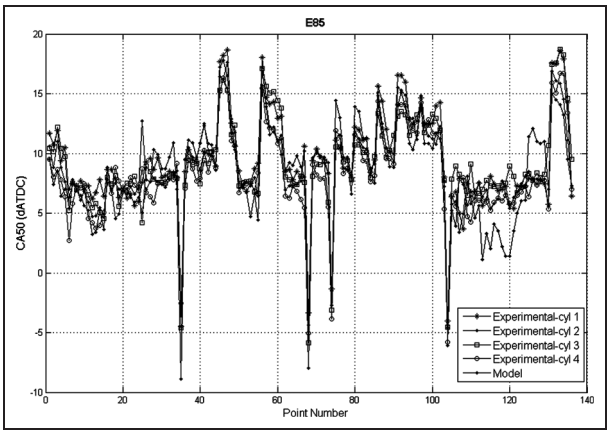

Figure 18. Model prediction of CA50 with E85.

In summary and as demonstrated in Figures 10 and 11, the model is quite accurate for the vast majority of the operating conditions, BGFs and ethanol blends considered.

Sensitivity of CA50 to inputs

As demonstrated in the previous section, this physically based, generalizable model accurately predicts CA50 under a variety of different operating conditions. Therefore, the model can be used to investigate the influence of different inputs on the CA50 timing. Valve overlap and SIT are control inputs that affect the gas exchange and flame-propagation processes, while ethanol blend ratio can be considered a disturbance (uncontrolled input) to the system. In this section, the model will be utilized to study the influence of valve overlap, ethanol blend and spark timing on CA50.

Valve overlap affects the amount of burned gases present in the cylinder, as demonstrated in Figure 20 for E0. In regions of NVO, the effect of valve overlap on the BGF is negligible; however, when PVO is achieved, the BGF increases as PVO increases. This effect is different depending on the operating conditions. At some operating points, the intake and exhaust manifolds have similar pressures and the BGF is relatively constant, regardless of valve overlap. However, at other operating points, there is a larger pressure difference across the engine and the resulting BGFs can be significant (up to 25%), as shown in Figure 20.

Since valve overlap affects the BGF, it also influences the CA50 (equation (28)). As shown in Figure 21, CA50 increases as BGF increases due to the impact of BGF on flame speed, as captured by equation (30).

As described previously, increasing the ethanol blend fraction decreases CA50 due to the faster flame speeds of ethanol.[37,44,43,41] Since the equivalence ratio is kept at 1, increasing the ethanol blend also requires an increase in fuelling (due to the lower stoichiometric AFR of ethanol). Figure 22 demonstrates the impact of higher flame speeds (via equation (29)) on CA50 reduction. A change in ethanol blend from E0 to E85 can cause up to a 6° change in CA50.

The spark timing also directly affects the CA50 timing, since it dictates the start of the flame-propagation process. Earlier spark timings lead to earlier CA50s. Spark timing can be used to maintain an optimal CA50

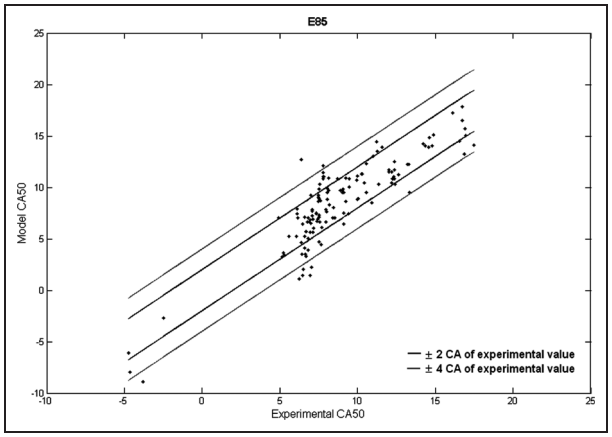

Figure 19. Comparison between experimental value and model prediction for CA50 with E85.

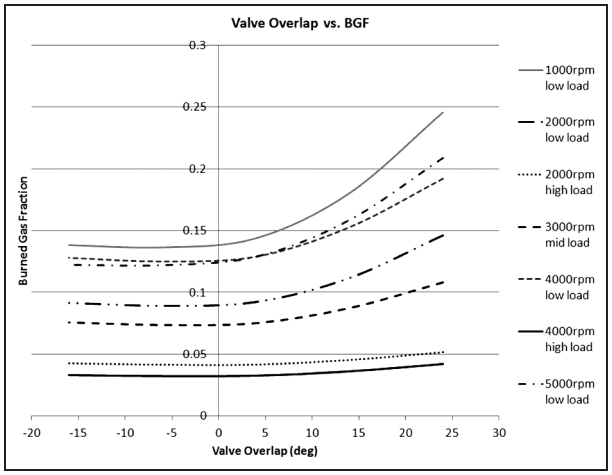

Figure 20. Impact of valve overlap on the in-cylinder BGF.

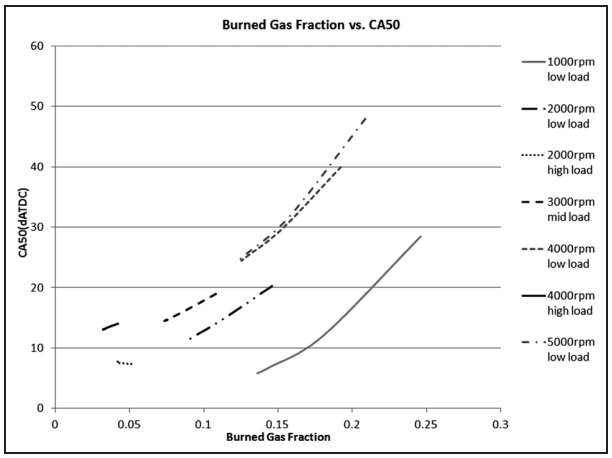

Figure 21. Impact of BGF on CA50 at different operating conditions.

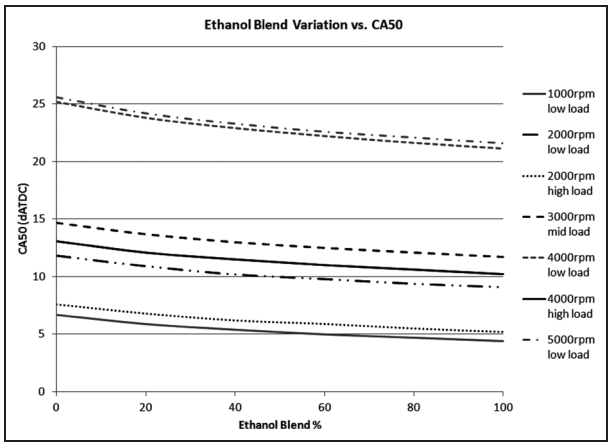

Figure 22. Impact of ethanol blend on CA50 at different operating conditions.

in the presence of BGF variation (due to changes in valve overlap), as well as changes in ethanol blend. Figure 23 demonstrates the variation in SIT required to keep CA50 at its optimal value (8 above TDC) when ethanol blend and valve overlap are introduced. As shown in Figure 23, BGF variation can alter the optimal spark timing by over 25° at some operating conditions, and ethanol content can change the optimal SIT by up to 6°. Therefore, it is crucial that both ethanol content and BGF variations be taken into account in SIT decision making.

The optimal SIT for varying values of valve overlap was also experimentally determined and compared to model results at several operating points with E0, E40, and E85 blends, as shown in Figures 24 and 25. While the model could be retuned so that better agreement is seen at these specific points, this would cause worsened performance in other operating conditions. However, Figures 24 and 25 demonstrate that not only are the trends for optimal SIT captured well, but the absolute values are also generally captured to within 2° CA of experimental values.

It is clear that valve overlap, as well as ethanol blend, can have an significant impact on the timing of CA50 as demonstrated in Figures 20 to 22. Optimal spark timings are substantially altered in the presence of ethanol content and BGF variation, as captured by Figure 23. The model predicts the optimal spark timing required to maintain an optimal timing for CA50.

Conclusions and future work

In this work, a combustion phasing model for fuel-flexible engines with VVT has been developed that is physically based and generalizable to different engine architectures. The model has been demonstrated to accurately capture changes in CA50 due to variation in thermodynamic conditions, valve overlap, spark advance and ethanol blend fraction at over 500 points across the engine operating range of a four-cylinder fuel-flexible SI engine with VVT. The model captures the rate of fuel burn from SIT to CA50 within 10% of the actual experimental values at a majority (over 90%)

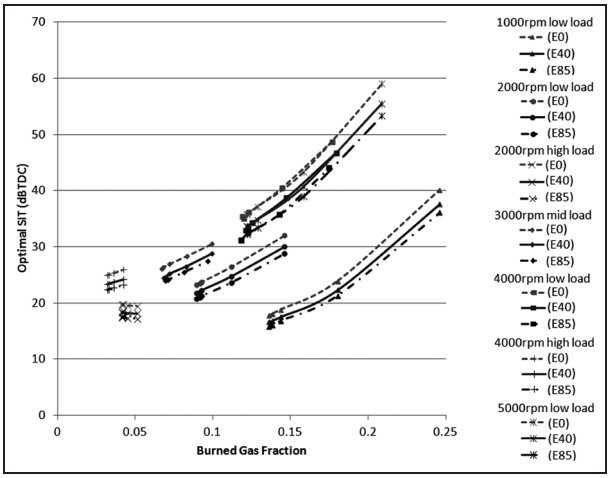

Figure 23. SIT required to obtain the optimal CA50 at different operating conditions.

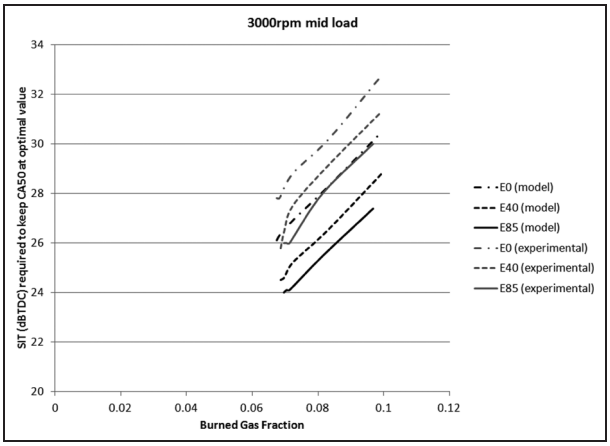

Figure 24. SIT required to obtain the optimal CA50 at different operating conditions.

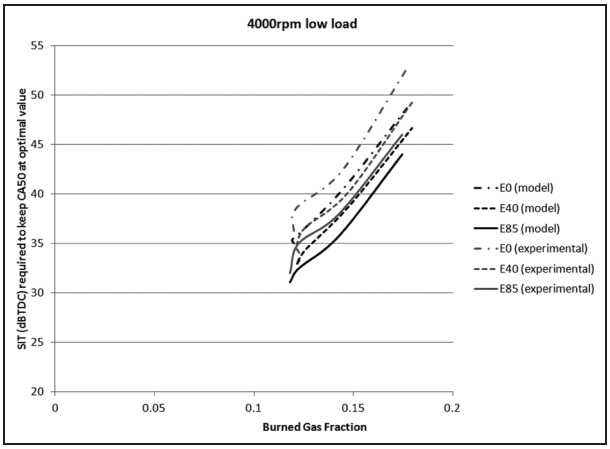

Figure 25. SIT required to obtain the optimal CA50 at different operating conditions.

of these points. Furthermore, its computational simplicity and the fact that it uses only available engine sensor measurements make it extremely valuable for efforts to control combustion phasing.

In current control methods, static look-up tables are used extensively for control of ignition, and while such tables provide acceptable control in steady state for their intended fuel, significant performance is lost during transients and when other alternative fuels are utilized. Since the model detailed in this paper can predict CA50 on a cycle-to-cycle basis for multiple fuels, it can be used to correct or replace the existing look-up tables. This could be done by comparing the estimated CA50 given by the model to a desired CA50 (which is typically known for an engine). The error between the desired and estimated CA50 can be used to drive feedback and feedforward control algorithms, which would adjust the spark advance timing to an optimal timing that provides the desired combustion phasing. Future efforts will focus on developing such control strategies in order to improve performance during transients and when operating with alternative fuels and VVT.

Funding

This work was supported by the National Science Foundation Graduate Research Fellowship [grant no. 103049 – award no. 0833366].

Acknowledgements

Special thanks to IFP Energies Nouvelles for providing experimental support on this project. The authors also wish to thank Lyle Kocher, Gayatri Adi, Thomas Leroy, and Thomas Coppin for their advice and contributions to this work.

References

1. Coppin T, Grondin O, Maamri N, and Rambault L. Fuel estimation and air-to-fuel ratio control for flexfuel spark-ignition engines. In: *2010 IEEE International Conference on Control Applications*, 2010.
2. Nakata K, Utsumi S, Ota A, Kawatake K, Kawai T, and Tsunooka T. The effect of ethanol fuel on a spark ignition engine. SAE paper 2006-01-3380, 2006.
3. Caton PA, Hamilton LJ, and Cowart JS. An experimental and modeling investigation into the comparative knock and performance characteristics of e85, gasohol[e10] and regular unleaded gasoline[87(r + m)/2]. SAE paper 2007-01-0473, 2007.
4. Cairns A, Todd A, ALeiferis P, Fraser N, and Malcolm J. A study of alcohol blended fuels in an unthrottled single cylinder spark ignition engine. SAE paper 2010-01-0618, 2010.
5. Coppin T, Grondin O, Le Solliec F, Rambault, and N. Maamri L. Control-oriented mean-value model of a fuel-flexible turbocharged spark-ignition engine. SAE paper 2010-01-0937, 2010.
6. Ahn K, Stefanopoulou A, and Jankovic M. Estimation of ethanol content in flex-fuel vehicles using an exhaust gas oxygen sensor: Model, tuning, and sensitivity. In:

2008 Proceedings of the ASME Dynamic Systems and Control Conference, pages 1309–1316, 2008.
7. Ahn K, Stefanopoulou A, and Jankovic M. Tolerant ethanol estimation in flex-fuel vehicles during MAF sensor drifts. In: *Proceedings of the ASME 2009 Dynamic Systems and Control Conference*, 2009.
8. Ahn K, Stefanopoulou A, and Jankovic M. Fuel puddle model and afr compensator for gasoline-ethanol blends in flex-fuel engines. In: *Proceedings of the IEEE Vehicle Power and Propulsion Conference*, 2009.
9. Heywood J. *Internal combustion engine fundamentals*. New York: McGraw-Hill, 1988.
10. Nakama K, Kusaka J, and Daisho Y. Effect of ethanol on knock in spark ignition gasoline engines. SAE paper 2008-32-0020, 2008.
11. Fontana G, Galloni E, Palmaccio R, and Torella E. The influence of variable valve timing on the combustion process of a small spark-ignited engine. SAE paper 2006-01-0445, 2006.
12. Cairns A, Todd A, Hoffman H, ALeiferis P, and Malcolm J. Combining unthrottled operation with internal EGR under port and central direct fuel injection conditions in a single cylinder SI engine. SAE paper 2009-01-1835, 2009.
13. Sher E and Bar-Kohany T. Optimization of variable valve timing for maximizing performance of an unthrottled SI engine – a theoretical study. *Energy*, 27:757–775, 2002.
14. Scharrer O, Heinrich C, Heinrich M, Gebhard P, and Pucher H. Review and analysis of variable valve timing strategies - eight ways to approach. SAE paper 2004-01-0614, 2004.
15. Hong H, Parvate-Patil GB, and Gordon B. Review and analysis of variable valve timing strategies - eight ways to approach. *Proc IMechE, Part D: J Automobile Engineering* 2004; 218: 1179–1200.
16. Cleary D and Silvas G. Unthrottled engine operation with variable intake valve lift, duration, and timing. SAE paper 2007-01-1282, 2007.
17. Song J and Sunwoo M. Flame kernal formation and propagation modelling in spark ignition engines. *Proc IMechE, Part D: J Automobile Engineering* 2001; 218: 105–114.
18. Bade Shrestha SO and Karim GA. A predictive model for gas fueled spark ignition engine applications. SAE paper 1999-01-3482, 1999.
19. Lafossas FA, Colin O, Le Berr F, and Menegassi P. Application of a new 1D combusiton model to gasoline transient engine operation. SAE paper 2005-01-2107, 2005.
20. Bougrine A, Richard S, and Veynante D. Modelling and simulation of the combustion of ethanol blended fuels in a SI engine using a 0D coherent flame model. SAE paper 2009-24-0016, 2009.
21. Richard S, Bougrine S, Font G, Lafossas FA, and Le Berr F. On the reduction of a 3D CFD combustion model to build a physical 0D model for simulating heat release, knock and pollutants in SI engines. *Oil Gas Sci Tech – Rev. IFP*, 64(3):223–242, 2009.
22. Le Berr F, Miche M, Le Solliec G, Lafossas FA, and Colin G. Modelling of a turbocharged SI engine with variable camshaft timing for engine control purposes. SAE paper 2006-01-3264, 2006.
23. Lee T-K, Kramer D, and Filipi Z. High-degree-of-freedom engine modelling for control design using a crank-angle-resolved flame propagation simulation and artificial neural network surrogate models. *J Syst Contr Eng* 2010; 224: 747–761.
24. Ahn K, Stefanopoulou AG, Jiang L, and Yilmaz H. Ethanol content estimation in flex fuel direct injection engines using in-cylinder pressure measurements. In: *SAE World Congress*, 2010.
25. Oliverio N, Stefanopoulou A, Jiang L, and Yilmaz H. Ethanol detection in flex-fuel direct injection engines using in-cylinder pressure measurements. SAE paper 2009-01-0657, 2009.
26. Theunissen FM. Percent ethanol estimation on sensorless multi-fuel systems: advantages and limitations. SAE paper 2003-01-3562, 2003.
27. Leroy T, Alix G, Chauvin J, Duparchy A, and Le Berr F. Modeling fresh air charge and residual gas fraction on a dual independent variable valve timing SI engine. SAE paper 2008-01-0983, 2008.
28. Leroy T. *Cylinder filling control of variable-valve-actuation equipped internal combustion engines*. PhD thesis, MINES Paris Tech, 2010.
29. Kocher L, Koeberlein E, Van Alstine D, Stricker K, and Shaver G. Physically-based volumetric efficiency model for diesel engines utilizing variable intake valve actuation. In: *2011 Dynamics Systems and Control Conference*, 2011.
30. Turns S. *An introduction to combustion*. New York: McGraw-Hill, 2000.
31. Hillion M, Chauvin J, and Petit N. Open-loop combustion timing control of a spark-ignited engine. In: *Proceedings of the 47th IEEE Conference on Decision and Control*, 2008.
32. Hillion M. *Transient combustion control of internal combustion engines*. PhD thesis, MINES Paris Tech, 2009.
33. Koeberlein E, Kocher L, Van Alstine D, Stricker K, and Shaver GM. Physics-based control-oriented modeling of exhaust gas enthalpy for engines utilizing variable valve actuation. In: *2011 Dynamic Systems and Control Conference Proceedings*, 2011.
34. Prucka R, Lee T, Filipi Z, and Assanis D. Turbulence intensity calculation from cylinder pressure data in a high degree of freedom spark-ignition engine. SAE paper 2010-01-0175, 2010.
35. Hiroyasu H and Kadota T. Computer simulation for combustion and exhaust emisssions on spark-ignition engine. In: *15th Symposium (International) on Combustion*, pages 1213–1233, 1975.
36. Ramos J. *Internal combustion engine modeling*. New York: Hemisphere Publishing Corporation, 1989.
37. Bayraktar H. Experimental and theoretical investigation of using gasoline-ethanol blends in spark-ignition engines. *Ren Energy*, 30:1733–1747, 2005.
38. Gülder O. Laminar burning velocities of methanol, ethanol, isooctane-air mixtures. In: *19th Symposium (International) on Combustion*, pages 275–281, 1982.
39. Metghalchi M and Keck J. Burning velocities of mixtures of air with methanol, isooctane and indolene at high pressure and temperature. *Comb Flame*, 48:191–210, 1982.
40. Bonatesta F and Shayler P. Factors influencing the burn rate characteristics of a spark ignition engine with variable valve timing. *Proc IMechE, Part D: J Automotobile Engineering*, 222(11):2147–2158, 2008.

41. Syed I, Yeliana, Mukherjee A, Naber J, and Michalek D. Numerical investigation of laminar flame speed of gasoline-ethanol/air mixtures with varying pressure, temperature, and dilution. SAE paper 2010-01-0620, 2010.
42. Lindström F, Ångström H, Kalghatgi G, and Möller C. An emperical SI combustion model using laminar burning velocity correlations. SAE paper 2005-01-2106, 2005.
43. Gülder OL. Correlations of laminar combustion data for alternative s.i. engine fuels. SAE paper 8410000, 1984.
44. Broustail G, Seers P, Halter F, Morèac G, and Mounaim-Rousselle C. Experimental determination of laminar burning velocity for butanol and ethanol iso-octane blends. *Fuel*, 90:1–6, 2011.
45. Hara T and Tanoue K. Laminar flame speed of ethanol, n-heptane, iso-octane air mixtures. JSAE paper 20068518, 2006.

Appendix 1

Notation

$\bar{A}$	mean flame area
amb	ambient
b	burned
bg	burned gas
E	energy
f	turbulence-enhancement factor
h	enthalpy
m_{fuel}	mass of fuel burned
M	mass
M_{fresh}	fresh air mass
M_{fuel}	injected fuel mass
n	polytropic coefficient
N	engine speed
P	pressure
Q	heat
Q_{LHV}	lower heating value
res	residual
r_{flame}	flame radius
R	universal gas constant
T	temperature
u	unburned
U	internal energy
U_L	laminar flame speed
U_{turb}	turbulent flame speed
V	volume
W	work
x_{fuel}	mass fraction of burned fuel
Y_{bg}	burned gas fraction
$Y_{fuel,u}$	mass fraction of fuel in the unburned zone
γ	ratio of the heat capacity at constrant pressure to heat capacity at constant volume
δI	distance between cylinder head and piston
ϕ	equivlance ratio
ρ_u	density in the unburned zone

Applitions

AFR	air-fuel ratio
BGF	burned gas fraction
CA	crank angle
CA50	CA when 50% of the fuel has burned
E0	gasoline
E5	5% ethanol/95% gasoline
E40	40% ethanol/60% gasoline
E85	85% ethanol/15% gasoline
EGR	exhaust gas recirculation
EM	exhaust manifold
EVC	exhaust valve closing
EVO	exhaust valve opening
IM	intake manifold
IVC	intake valve closing
IVO	intake valve opening
NVO	negative valve overlap
OF	overlap factor,
PVO	positive valve overlap
SI	spark ignition
SIT	SI timing
TDC	top dead center
VVT	variable valve timing

Appendix 2

Summary of model input variation

Figure 26 shows the variation in speed, intake and exhaust manifold temperature and pressure, fresh air mass, spark advance, and valve overlap at the E0 points. These are the inputs to the engine cylinder that affect the gas exchange and compression processes, as shown in Figure 4. The engine speed affects the amount of turbulence in-cylinder (equation (30)). The intake and exhaust pressures will affect the gas exchange process by directly impacting the mass of fresh (equation (1)) and burned gases (equations (2) and (5)). Higher intake pressures are indicative of higher load conditions on the engine (which require higher air and fuel flows). While the intake temperatures are approximately constant, the exhaust temperature varies more substantially depending on the engine load. These exhaust temperature changes impact the burned gas mass (equations (2) and (5)), as well as the temperature at IVC (equation (9)). The fresh air mass is typically higher for higher loads and both the trends and absolute values are captured well by the fresh air submodel (equation (1)). Spark timing is also significantly varied and directly impacts a number of inputs to the flame-propagation model. Valve overlap also affects the mass of burned gases. As valve overlap increases and BGF increases, flame speeds are slowed and earlier spark timing is required to maintain the same CA50. These cylinder inputs are used in the gas exchange and compression models. Following these phases, the initial conditions to the flame-propagation model (Figure 4) are calculated to be those shown in Figure 27. The fuel mass fraction, in-cylinder pressure, temperature, volume, density, BGF and equivalence ratio all impact the speed at

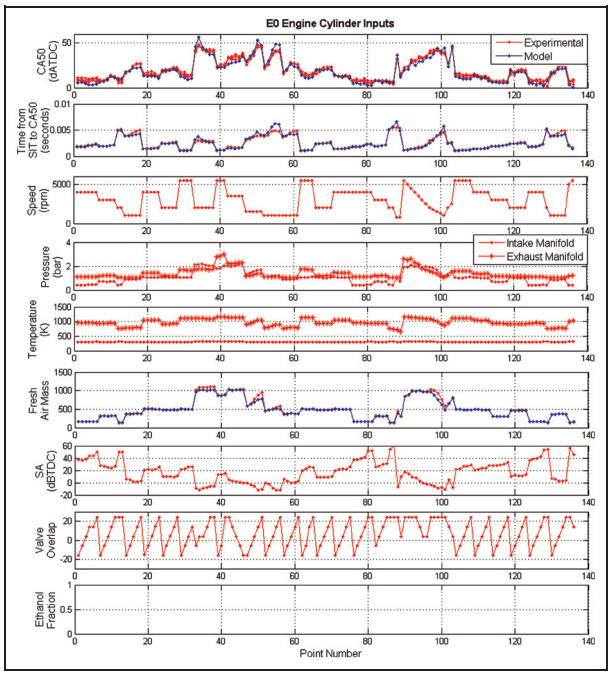

Figure 26. Inputs to the model for E0 data set.

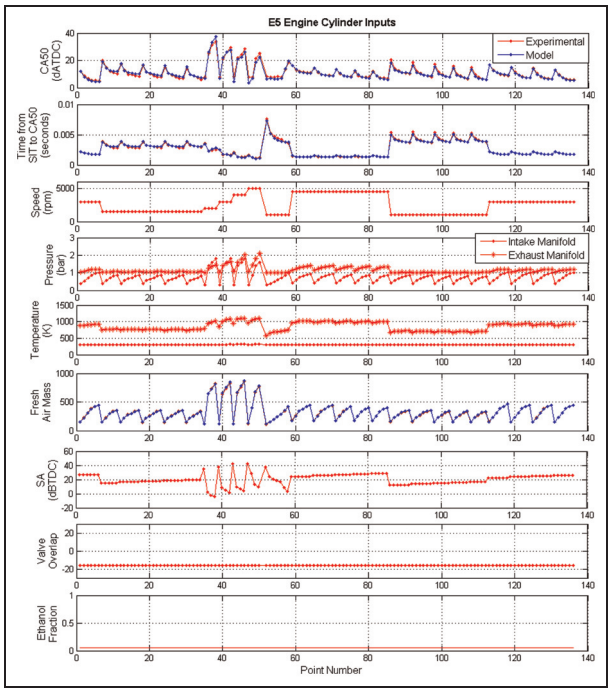

Figure 28. Inputs to the model for E5 data set.

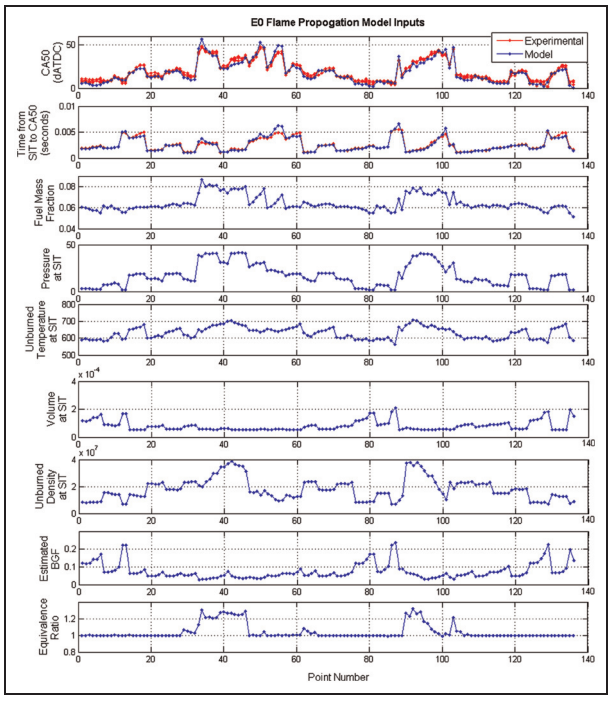

Figure 27. Inputs to the flame-propagation model for E0.

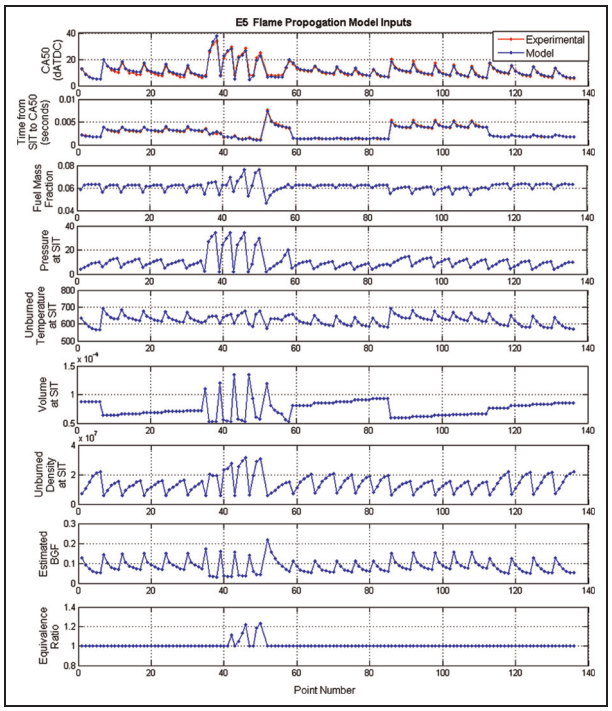

Figure 29. Inputs to the flame-propagation model for E5.

which the flame propagates. Higher temperatures, pressures, and densities speed up the fuel burn rate as captured in equation (31). Increases in BGF due to changes in valve overlap slow down the flame propagation. The equivalence ratio for a majority of these points is controlled to be 1, indicating stoichiometric combustion as expected for an SI engine; however, at some high loads, it becomes necessary to run rich of stoichiometric in order to prevent exhaust temperatures from becoming excessively high and avoid knock.[5,9] Figure 28 shows the variation in speed, intake and exhaust manifold temperature and pressure, fresh air mass, spark advance and valve overlap for the E5 data set. Note that in all cases, valve overlap is at its minimum. While valve overlap is constant, the BGF still changes due to variation in the exhaust temperatures and pressures (equation (2)). The flame-propagation model inputs are shown in Figure 29.

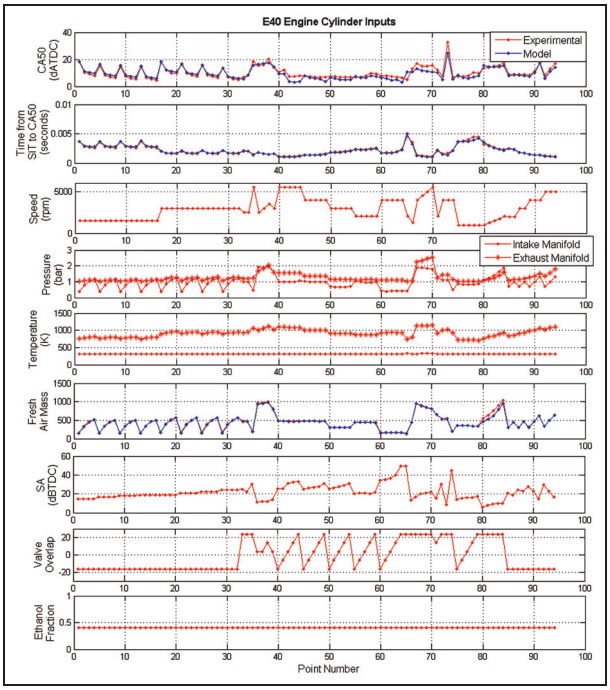

Figure 30. Inputs to the model for E40 data set.

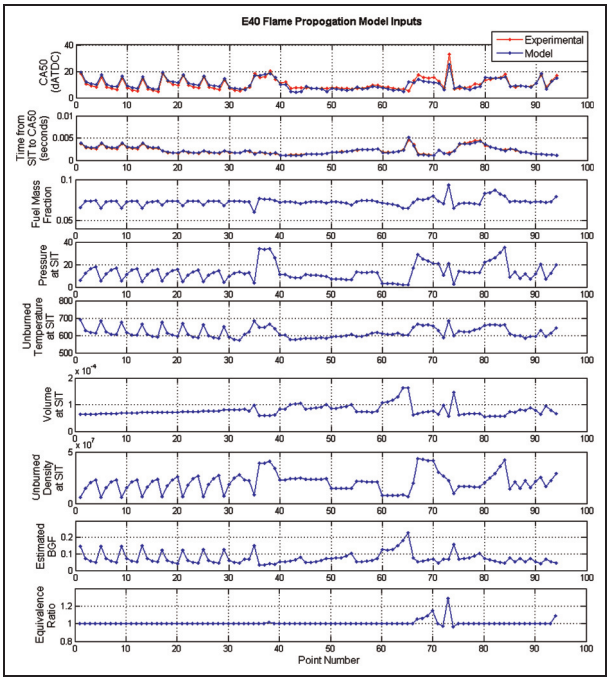

Figure 31. Inputs to the flame-propagation model for E40.

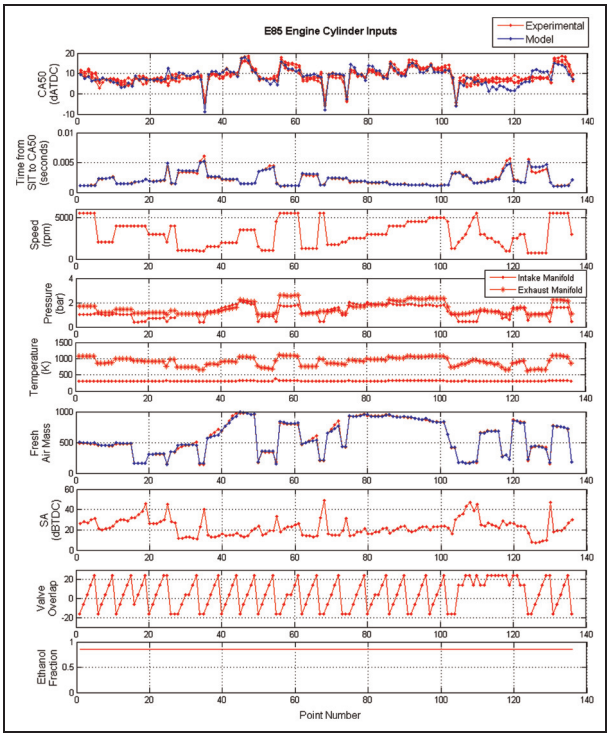

Figure 32. Inputs to the model for E85 data set.

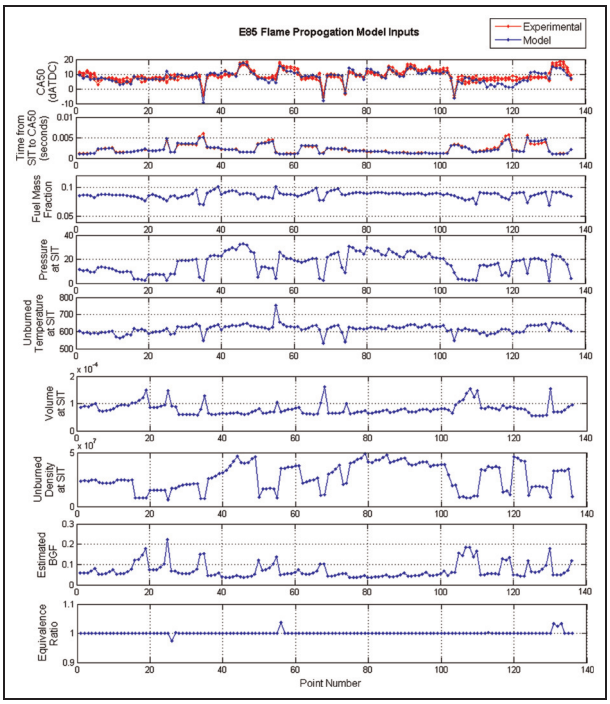

Figure 33. Inputs to the flame-propagation model for E85.